Development and characterization of powder metallurgically produced discontinuous tungsten fiber reinforced tungsten composites

Y.Mao[a], J.W.Coenen[a], J.Riesch[b], S.Sistla[c], J.Almanstötter[d], B.Jasper[a], A.Terra[a], T.Höschen[b], H.Gietl[b,e], M. Bram[f], J. Gonzalez-Julian[f], Ch.Linsmeier[a] and Ch.Broeckmann[c]

[a] Institut für Energie und Klimaforschung – Plasmaphysik, Forschungszentrum Jülich GmbH, 52425 Jülich, Germany

[b] Max-Planck-Institut für Plasmaphysik, 85748 Garching b. München, Germany

[c] Institut für Werkstoffanwendungen im Maschinenbau (IWM), RWTH Aachen University, 52062 Aachen, Germany

[d]OSRAM GmbH, SP PRE PLM DMET, Mittelstetter Weg 2, 86830 Schwabmünchen, Germany

[e]Technische Universität München, Boltzmannstrasse 15, 85748 Garching, Germany

[f] Institut für Energie und Klimaforschung - Materials Synthesis and Processing, Forschungszentrum Jülich GmbH, 52425 Jülich, Germany

Abstract: In future fusion reactors, tungsten is the prime candidate material for the plasma facing components. Nevertheless, tungsten is prone to develop cracks due to its intrinsic brittleness – a major concern under the extreme conditions of fusion environment. To overcome this drawback, tungsten fiber reinforced tungsten (W_f/W) composites are being developed. These composite materials rely on an extrinsic toughing principle, similar to those in ceramic matrix composite, using internal energy dissipation mechanisms, such as crack bridging and fiber pull-out, during crack propagation. This can help W_f/W to facilitate a pseudo-ductile behavior and allows an elevated damage resilience compared to pure W. For pseudo-ductility mechanisms to occur, the interface between the fiber and matrix is crucial.

Recent developments in the area of powder-metallurgical W_f/W are presented. Two consolidation methods are compared. Field assisted sintering technology (FAST) and hot isostatic pressing (HIP) are chosen to manufacture the Wf/W composites. Initial mechanical

tests and microstructural analyses are performed on the Wf/W composites with a 30 % fiber volume fraction. The samples produced by both processes can give pseudo-ductile behavior at room temperature.

1. Introduction

Tungsten is currently the main candidate material for plasma facing component in future fusion reactors due to its resistance against erosion, high melting point, low tritium retention and benign activation behavior by neutron irradiation [1, 2]. However, its application is strongly restricted by its inherent brittleness. Under the extreme conditions of fusion environment with high transient heat loads and neutron irradiation, a tungsten plasma facing material will face the possibility of crack formation during operation and subsequent catastrophic failure [3]. Tungsten fiber reinforced tungsten (W_f/W) composites have been developed to overcome this issue, relying on extrinsic toughing mechanisms by using commercially available tungsten wires as reinforcement [4-6]. By incorporation of the fibers, some local energy dissipation mechanism during crack propagation can be realized, such as fiber pull-out, ductile deformation of the fibers, crack deflection and interface de-bonding. These mechanisms enable W_f/W to behave pseudo ductile [7], similar to ceramic matrix composites [8-10]. The crucial factor to realize pseudo ductility is the existence of a relatively weak fiber-matrix interface [11-13].

The two potential methods to manufacture W_f/W composites are chemical vapor deposition (CVD) [7, 14] and powder metallurgy processes (PM) [15-18]. Both production routes have shown the possibility to achieve the expected pseudo ductility. Compared to the CVD production route, the PM process, as a more standard industrial process, has several benefits, such as substantial experience with bulk production, higher sample density and an easier

realization of alloy production. However, the potential issue of the PM process is that, the high temperature during sintering will cause recrystallization of the tungsten fiber and, hence, weaken the fibers ductility and strength [5, 19]. Additionally, the fiber-matrix interface will be damaged during the sintering process due to the high temperature and pressure [15, 20].

In this work, as introducing long fibers into the PM processes is technically difficult, discontinuous tungsten fibers (2.4 mm length) are chosen to reinforce the tungsten matrix. The samples were prepared via different PM processes: Field assisted sintering technology (FAST) [21-25] and hot isostatic pressing (HIP) [26-28]. The study focuses on the microstructure and load capability of the PM produced W_f/W.

2. W_f/W manufacturing and microstructure

The raw materials of the W_f/W composites fabrication are pure tungsten powders (provided by OSRAM GmbH) with 5 µm average particle size (fischer sub sieve size) and potassium doped short tungsten fibers (provided by OSRAM GmbH) with 2.4mm length and 0.24mm diameter. The tungsten fibers were produced by a drawing process and then cut into the required length. Due to the drawn microstructure with elongated grains, the tungsten fibers show ductile behavior and extremely high tensile strength (~3000 MPa) [5, 19]. Since potassium is insoluble in tungsten the doping (approx. 75 ppm) is present in form of nano-disperse rows of bubbles along the elongated grains pinning the grain boundaries and thus leading to a good high temperature microstructure stability [5].

As a first step of sample manufacturing, the tungsten fibers were coated with a 2.5 µm yttria layer to form a dedicated fiber-matrix interface, by using a magnetron sputtering process.

Coating production details are shown in [20]. Fig. 1 presents a scanning electron microscope (SEM) image of a typical yttria thin film cross section prepared by focused ion beam (FIB) cut.

In a next step, the tungsten fibers were mixed with the tungsten powders by manual shaking in a vessel with a fiber volume fraction of 30%. The similar density of the tungsten powders and the tungsten fibers leads to a random distribution of the tungsten fibers in the mixture.

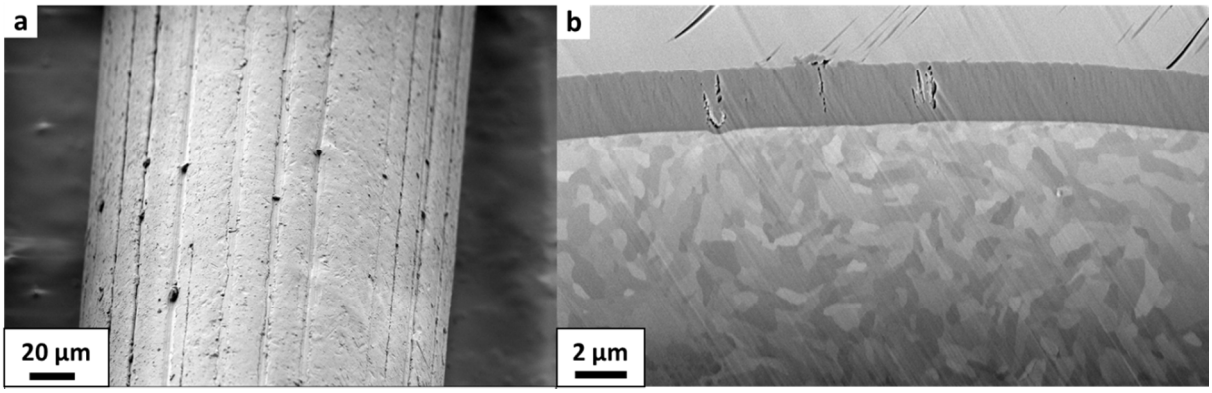

Fig: 1: Scanning electron microscope (SEM) image of the as-deposited yttrium oxide thin film surface on single tungsten fiber (a); SEM image of the thin film cross section prepared by focused ion beam (FIB) cut showing yttrium oxide thin film structure (b) (the visible additional top layer of platinum was deposited during sample preparation for FIB cut).

Afterwards, the fiber-powder mixture was sintered (consolidated) by a FAST or HIP process, respectively. The FAST and HIP process parameters are shown in Table 1.

Schematic diagrams of the processes are shown in Fig. 2. During the FAST process, the powder-fiber mixture was consolidated in a graphite die with 20 mm inner diameter. The sintering was performed under vacuum below 0.1 mbar. Tungsten powder and fiber mixture were then heated by current Joule heating through the sample under high uniaxial pressure (in z direction) [29]. As result, coin shape samples (20 mm diameter and ~5 mm height) was produced (Fig. 3).

For the HIP process, the powder/fiber mixture was firstly uniaxial (in z direction in Fig .2) pre-pressed at 200 MPa and then put into a tantalum capsule. After vacuum seal welding, the tantalum capsule was then consolidated in the HIP chamber. The isostatic pressure was applied by means of an Argon gas inlet. The HIP sample after consolidation is cylindrical in shape with ~18 mm diameter and ~14 mm height (Fig. 3).

The mass density of the sintered W_f/W samples after consolidation was measured by the Archimedes principle. The results are given in Table. 1.

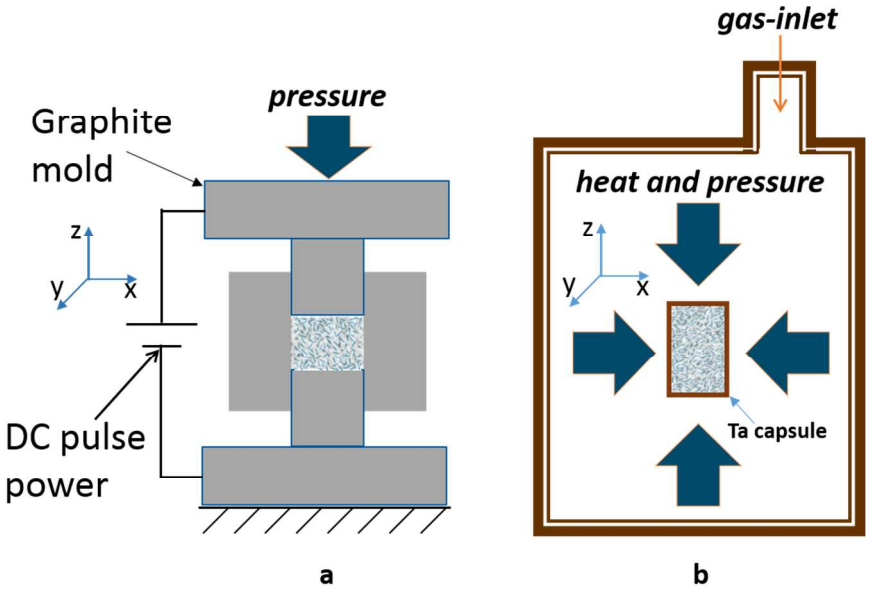

Fig. 2: Schematic diagram of FAST (a) and HIP (b) processes.

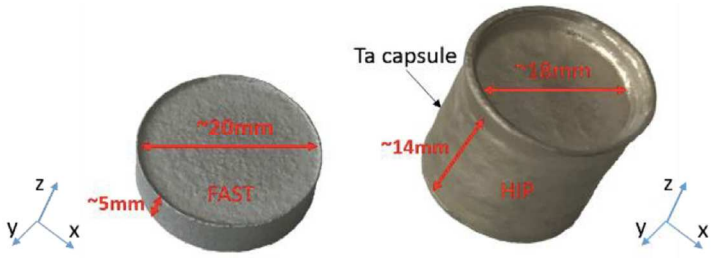

Fig. 3: Representative W_f/W samples after powder metallurgical consolidation.

	Temperature	Pressure	Holding time	Heating rate	Relative density
FAST	1900 °C	60 MPa	4 min	200 K/min	~94%
HIP	1600 °C	200 MPa	2 h	10 K/min	~98%

Table. 1: FAST and HIP process parameters and relative density of the samples.

Fig. 4 and 5 represent an overview of the typical microstructure of the as-fabricated W_f/W samples for both fabrication process respectively. The cross sections shown are parallel and perpendicular to z axis, respectively. A relatively homogeneous fiber distribution can be observed in all cases. Potential fiber distribution inhomogeneity (areas marked by dash lines in Fig. 4 and 5) could be caused by insufficient shaking during mixing or punch/capsule compression during sintering.

The samples from both processes tend to have a 2-dimentional planar fiber orientation distribution. Most fibers tend to orient parallel to x-y plane. For the FAST process, it is assumed to be due to the height reduction in the z-direction during sintering. For the HIP process, it is caused by the uniaxial pre-pressing (in z direction) during green body preparation. Additionally, fiber deformation after consolidation is visible, especially when fibers are in contact with each other, as marked by solid circles in Fig. 5.

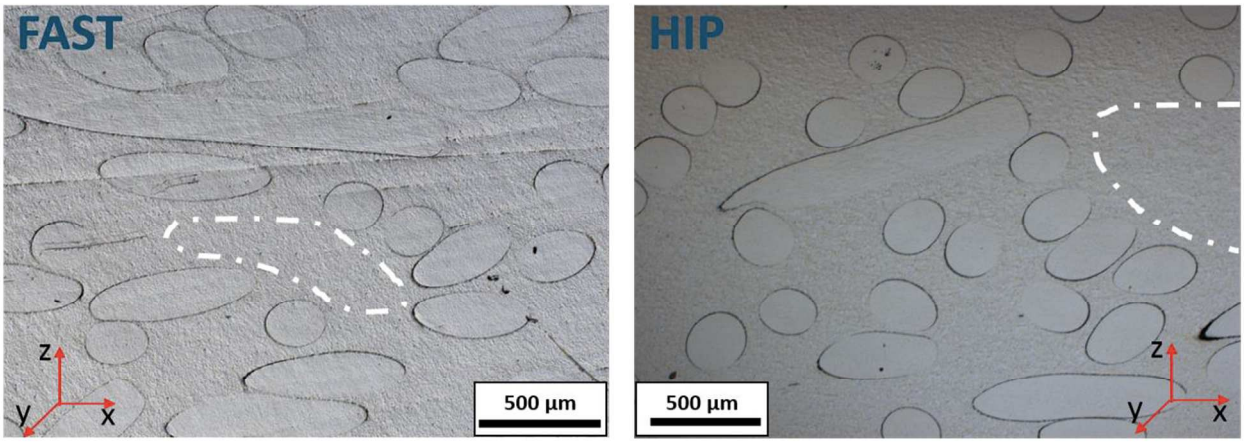

Fig. 4: Light microscope image of the overview microstructure of the FAST and HIP produced W_f/W, the cross sections are parallel to z axis. The dash lines mark the potential inhomogeneous fiber distribution areas.

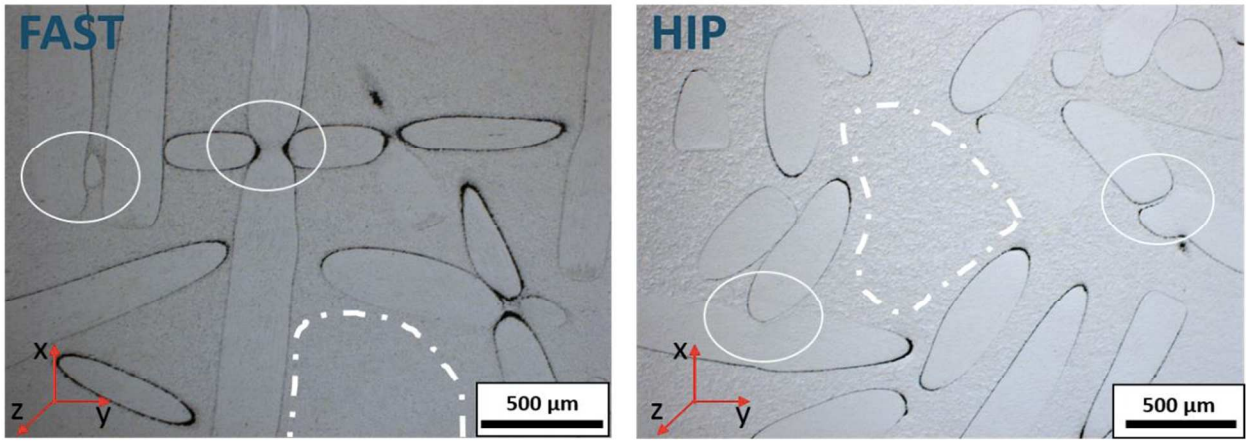

Fig. 5 Light microscope image of the overview microstructure of the FAST and HIP produced W_f/W, the cross sections are perpendicular to z axis. The dash lines mark the potential inhomogeneous fiber distribution areas and the solid circles mark the fiber deformation positions.

Fig. 6 represents the detailed view of the fiber-matrix interface region. An energy dispersive X-ray spectroscopy (EDX) mapping analysis was performed to detect local interface chemical composition. The location of elemental yttrium signal are shown in green. The fiber-matrix interfaces are visible after sintering for the samples from both processes. In contrast to the

dense and homogenous yttria layer in the as-coated (cf Fig. 1), the yttria interface show damage after the consolidation process. Especially the outer shell of the interface got penetrated by the tungsten powders owing to the external pressure and the high temperature [15, 20, 30, 31]. The interface damage during the FAST product looks, at a first glance, more severe (Fig. 6). We can see from the EDX results, in the FAST W_f/W, more yttria particles diffused into the matrix and the diffusion distance is larger. This is probably due to the higher process temperature. Also an effect called dielectric breakdown effect might play a role [30, 31], as yttria is electrically isolating.

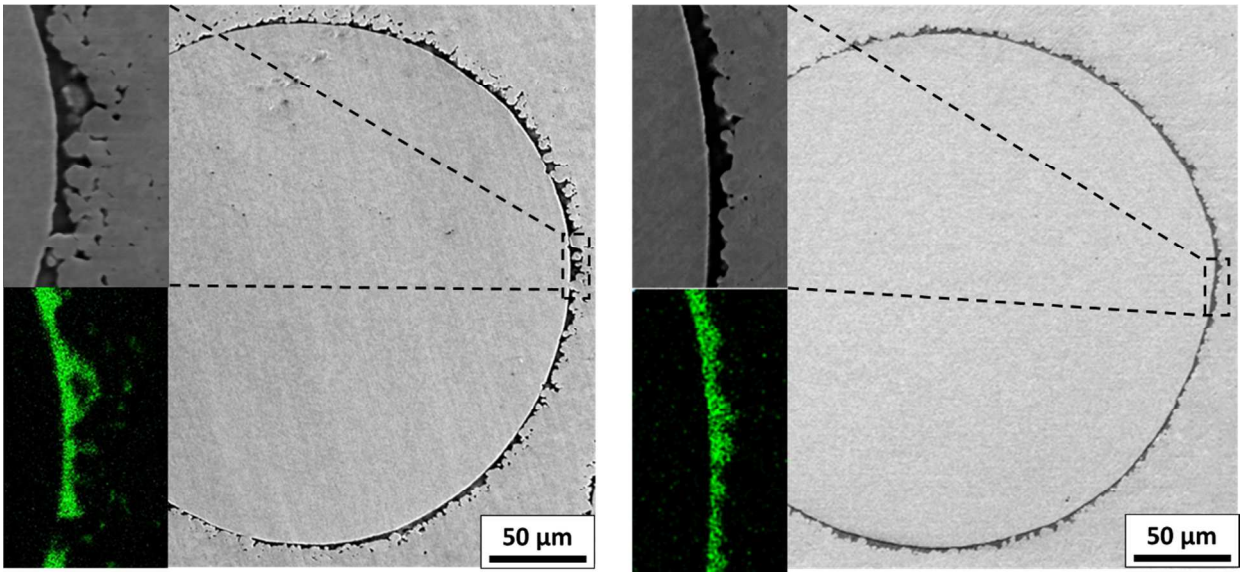

Fig. 6: SEM images of the Fiber-matrix interface region of the FAST and HIP produced W_f/W composites. An energy dispersive X-ray spectroscopy mapping analysis was performed. The location of elemental yttrium signal are shown in green.

3. Fracture behavior

To observe the crack propagation behavior of the W_f/W composites, a pre-notched 3-point bending test was performed at room temperature (RT) on samples produced by the above described processes. Sample dimensions were 18 x 2 x 4 mm^3 (length x width x thickness) with a

~2 mm deep notch. The pre-notch was prepared by diamond wire cutting followed by manually razor blade polishing. The bending tests were performed with an Instron 3342 universal testing machine (Instron GmbH, Darmstadt, Germany) with a displacement rate of 5 µm/s.

Typical load-displacement curves of pure W and W_f/W composites produced by FAST, as well as W_f/W composites produced by HIP are presented in Fig. 7. It is important to note that, the absolute force values in these curves are not directly comparable. Because the pre-notch was manually prepared, therefore, the sharpness and the depth of the notches are not identical. The fracture surfaces of the samples after the pre-notched 3-point bending tests are shown in Fig. 8.

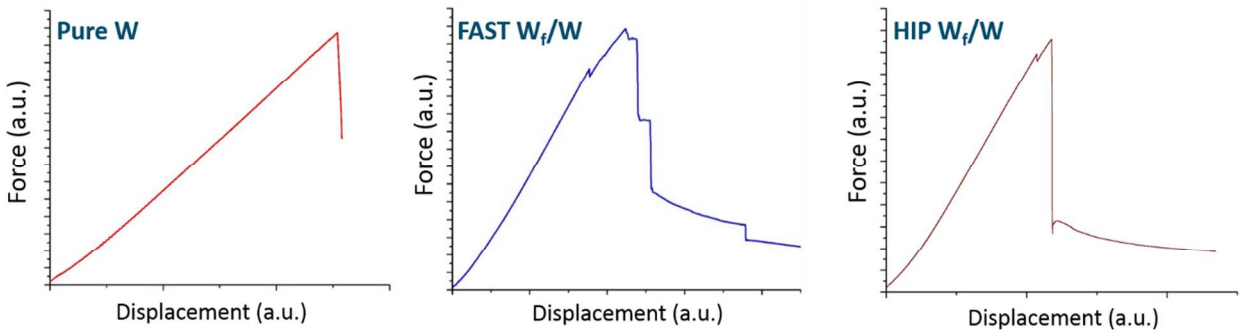

Fig. 7: Typical load-displacement curves of FAST produced pure W, W_f/W and HIP produced W_f/W during pre-notched 3-point bending tests.

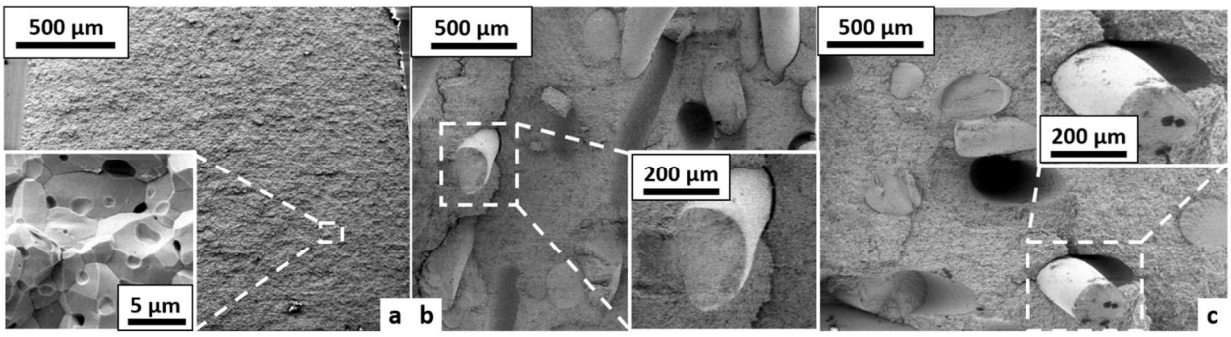

Fig. 8: SEM image of the fracture sections after the pre-notched 3-point bending tests of FAST produced pure W (a), W_f/W (b) and HIP produced W_f/W (c).

As shown in Fig, 7a, at RT, the pure tungsten sample show pure linearly elastic loading until a severe load drop to zero during failure without having any plastic deformation. Also a clear brittle intergranular fracture surface is observed as shown in Fig. 8a.

Both W_f/W samples give different force-displacement curves: after the first load-drop, the load still increases; a massive load-drop occurs after reaching the maximum load; afterwards, the samples tend to have a stepwise or continuous load-drop instead of a completely failure.

The matrix of the composites exhibits also intergranular fracture, similar to pure W. Interface de-bonding, fiber pull-out can be observed in both cases, as shown in Fig. 8b and c. Additionally, the overall fracture surface of the W_f/W is more uneven compared to the pure tungsten.

The above results give a strong indication that the PM produced W_f/W composites are able to exhibit typical pseudo ductile behavior similar to W_f/W produced by CVD [4]: the first load-drop signifies the matrix failure; after the matrix failure, the load still increases due to the crack bridging by the fibers; the massive load-drop indicates the multiple fiber failure; then the stepwise load bearing capability is probably supplied by frictional fiber pull-out from the matrix. The uneven fracture surface gives a hint for observed crack deflection. Here the fiber pull-out, fiber elastic bridging and crack deflection are likely the energy dissipation mechanisms which contribute to the elevated fracture resistance compared to pure tungsten [9, 32].

Additionally, with respect to the fracture behavior, some difference between FAST and HIP samples can be identified. The main difference is after maximum loading: for FAST sample, the load drop is more continuous (has more steps); for HIP sample, there is a sudden load drop to a low value. We expect this difference is caused by the different fiber-matrix interface strength. For FAST samples, in some regions, the fiber and matrix get sintered together, as we can see

from Fig. 6. In this case the bonding between fiber and matrix will be very strong and we can consider it like a tungsten/yttria mixed interface, instead a clean yttria interface. So the fiber-matrix interface strength is higher for FAST produced W_f/W. During the pull-out stage after multiple fiber failure, a higher strength interface could dissipate more energy (fiber-matrix friction is higher) so we end up with a more continuous load decreasing compared to HIP sample with a relatively low interface strength. The interface strength influence on W_f/W fracture behavior will be reported in future study.

4. Conclusion and outlook

W_f/W composites with ~94% and ~98% density are produced by FAST and HIP processes, respectively. Both processes give similar microstructures after consolidation with a relatively homogeneous fiber distribution. Fibers tend to have a 2-dimentional planar orientation. The Fiber-matrix interface remains intact after PM processes. The PM produced W_f/W samples are able to show a pseudo-ductility behavior at RT. This is in contrast to complete brittle behavior of pure tungsten. The improved resistance against fracture relies on energy dissipation mechanisms, such as fiber pull-out, crack bridging by the fibers and crack deflection. For the first time, pseudo ductile behavior of a HIP produced W_f/W composite at RT was presented.

The fiber volume fraction influence on the composite properties has also been studied and will be reported in the future. In the next step, the influence of the fiber-matrix interface strength on the composite will be studied. The W_f/W composites with different interface materials will be produced and analyzed. Standard fracture toughness measurements together with a microstructure study will be performed.

Acknowledgement: This work has been carried out within the framework of the EUROfusion Consortium and has received funding from the Euratom research and training program 2014-2018 under grant agreement No 633053. The views and opinions expressed herein do not necessarily reflect those of the European Commission. We would like to also thank Anna Weddeling from Lehrstuhl für Werkstofftechnik Ruhr-Universität Bochum for the assistance with the HIP process.

Reference

[1] V. Philipps, Tungsten as material for plasma-facing components in fusion devices, J. Nucl. Mater., 415 (2011) S2-S9.
[2] J.W. Coenen, S. Antusch, M. Aumann, W. Biel, J. Du, J. Engels, S. Heuer, A. Houben, T. Hoeschen, B. Jasper, F. Koch, J. Linke, A. Litnovsky, Y. Mao, R. Neu, G. Pintsuk, J. Riesch, M. Rasinski, J. Reiser, M. Rieth, A. Terra, B. Unterberg, W. Th, T. Wegener, J.H. You, L. Ch, Materials for DEMO and reactor applications—boundary conditions and new concepts, Physica Scripta, 2016 (2016) 014002.
[3] G. Pintsuk, I. Bobin-Vastra, S. Constans, P. Gavila, M. Rödig, B. Riccardi, Qualification and post-mortem characterization of tungsten mock-ups exposed to cyclic high heat flux loading, Fusion Engineering and Design, 88 (2013) 1858-1861.
[4] J. Riesch, T. Höschen, C. Linsmeier, S. Wurster, J.H. You, Enhanced toughness and stable crack propagation in a novel tungsten fibre-reinforced tungsten composite produced by chemical vapour infiltration, Physica Scripta, T159 (2014) 014031.
[5] J. Riesch, Y. Han, J. Almanstötter, J.W. Coenen, T. Höschen, B. Jasper, P. Zhao, C. Linsmeier, R. Neu, Development of tungsten fibre-reinforced tungsten composites towards their use in DEMO - Potassium doped tungsten wire, in: Physica Scripta, 2016.
[6] R. Neu, J. Riesch, J.W. Coenen, J. Brinkmann, A. Calvo, S. Elgeti, C. García-Rosales, H. Greuner, T. Hoeschen, G. Holzner, F. Klein, F. Koch, C. Linsmeier, A. Litnovsky, T. Wegener, S. Wurster, J.H. You, Advanced tungsten materials for plasma-facing components of DEMO and fusion power plants, Fusion Engineering and Design, 109-111 (2016) 1046-1052.
[7] H. Gietl, J. Riesch, J.W. Coenen, T. Höschen, C. Linsmeier, R. Neu, Tensile deformation behavior of tungsten fibre-reinforced tungsten composite specimens in as-fabricated state, Fusion Engineering and Design, (2017).
[8] K.K. Chawla, Ceramic matrix composites, in: Composite Materials, Springer, 1998, pp. 212-251.
[9] H. Stang, S.P. Shah, Failure of fibre-reinforced composites by pull-out fracture, Journal of Materials Science, 21 (1986) 953-957.

[10] V.C. Li, Y. Wang, S. Backer, A micromechanical model of tension-softening and bridging toughening of short random fiber reinforced brittle matrix composites, J. Mech. Phys. Solids, 39 (1991) 607-625.
[11] J. Du, T. Höschen, M. Rasinski, J.H. You, Shear debonding behavior of a carbon-coated interface in a tungsten fiber-reinforced tungsten matrix composite, J. Nucl. Mater., 417 (2011) 472-476.
[12] J. Du, T. Höschen, M. Rasinski, S. Wurster, W. Grosinger, J.H. You, Feasibility study of a tungsten wire-reinforced tungsten matrix composite with ZrOx interfacial coatings, Composites Science and Technology, 70 (2010) 1482-1489.
[13] J. Du, T. Höschen, M. Rasinski, J.H. You, Interfacial fracture behavior of tungsten wire/tungsten matrix composites with copper-coated interfaces, Materials Science and Engineering: A, 527 (2010) 1623-1629.
[14] J. Riesch, M. Aumann, J.W. Coenen, H. Gietl, G. Holzner, T. Höschen, P. Huber, M. Li, C. Linsmeier, R. Neu, Chemically deposited tungsten fibre-reinforced tungsten – The way to a mock-up for divertor applications, Nuclear Materials and Energy, 9 (2016) 75-83.
[15] J.W. Coenen, Y. Mao, J. Almanstötter, A. Calvo, S. Sistla, H. Gietl, B. Jasper, J. Riesch, M. Rieth, G. Pintsuk, F. Klein, A. Litnovsky, A.V. Mueller, T. Wegener, J.H. You, C. Broeckmann, C. Garcia-Rosales, R. Neu, C. Linsmeier, Advanced materials for a damage resilient divertor concept for DEMO: Powder-metallurgical tungsten-fibre reinforced tungsten, Fusion Engineering and Design, in press.
[16] B. Jasper, J.W. Coenen, J. Riesch, T. Höschen, M. Bram, C. Linsmeier, Powder Metallurgical Tungsten Fiber-Reinforced Tungsten, Materials Science Forum, 825-826 (2015) 125-133.
[17] B. Jasper, S. Schoenen, J. Du, T. Hoeschen, F. Koch, C. Linsmeier, R. Neu, J. Riesch, A. Terra, J.W. Coenen, Behavior of tungsten fiber-reinforced tungsten based on single fiber push-out study, Nuclear Materials and Energy, (2016).
[18] L.H. Zhang, Y. Jiang, Q.F. Fang, T. Zhang, X.P. Wang, C.S. Liu, Toughness and microstructure of tungsten fibre net-reinforced tungsten composite produced by spark plasma sintering, Materials Science and Engineering: A, 659 (2016) 29-36.
[19] J. Riesch, J. Almanstötter, J.W. Coenen, M. Fuhr, H. Gietl, Y. Han, T. Höschen, C. Linsmeier, N. Travitzky, P. Zhao, R. Neu, Properties of drawn W wire used as high performance fibre in tungsten fibre-reinforced tungsten composite, IOP Conference Series: Materials Science and Engineering, 139 (2016) 012043.
[20] Y. Mao, J. Engels, A. Houben, M. Rasinski, J. Steffens, A. Terra, C. Linsmeier, J.W. Coenen, The influence of annealing on yttrium oxide thin film deposited by reactive magnetron sputtering: Process and microstructure, Nuclear Materials and Energy, in press (2017).
[21] D.M. Hulbert, A. Anders, D.V. Dudina, J. Andersson, D. Jiang, C. Unuvar, U. Anselmi-Tamburini, E.J. Lavernia, A.K. Mukherjee, The absence of plasma in “spark plasma sintering”, J. Appl. Phys., 104 (2008) 033305.
[22] O. Guillon, J. Gonzalez-Julian, B. Dargatz, T. Kessel, G. Schierning, J. Räthel, M. Herrmann, Field-Assisted Sintering Technology/Spark Plasma Sintering: Mechanisms, Materials, and Technology Developments, Advanced Engineering Materials, 16 (2014) 830-849.
[23] Y. Kim, K.H. Lee, E.-P. Kim, D.-I. Cheong, S.H. Hong, Fabrication of high temperature oxides dispersion strengthened tungsten composites by spark plasma sintering process, International Journal of Refractory Metals and Hard Materials, 27 (2009) 842-846.

[24] K.N. Allahar, D.P. Butt, J. Webb, I. Charit, Electrochemical properties of spark plasma sintered tungsten, in: NACE - International Corrosion Conference Series, 2011.
[25] R. Ohser-Wiedemann, U. Martin, A. Müller, Fast sintering of mechanical alloyed Mo-W powders, in: Proceedings of the International Euro Powder Metallurgy Congress and Exhibition, Euro PM 2012, 2012.
[26] A.S. Helle, K.E. Easterling, M.F. Ashby, Hot-isostatic pressing diagrams: New developments, Acta Metall., 33 (1985) 2163-2174.
[27] A. Svoboda, H.A. Häggblad, L. Karlsson, Simulation of hot isostatic pressing of a powder metal component with an internal core, Computer Methods in Applied Mechanics and Engineering, 148 (1997) 299-314.
[28] E. Arzt, M.F. Ashby, K.E. Easterling, Practical applications of hotisostatic Pressing diagrams: Four case studies, Metallurgical Transactions A, 14 (1983) 211-221.
[29] R. Orrù, R. Licheri, A.M. Locci, A. Cincotti, G. Cao, Consolidation/synthesis of materials by electric current activated/assisted sintering, Materials Science and Engineering: R: Reports, 63 (2009) 127-287.
[30] C.S. Bonifacio, T.B. Holland, K. Van Benthem, Time-dependent dielectric breakdown of surface oxides during electric-field-assisted sintering, Acta Materialia, 63 (2014) 140-149.
[31] C.S. Bonifacio, T.B. Holland, K. van Benthem, Evidence of surface cleaning during electric field assisted sintering, Scripta Materialia, 69 (2013) 769-772.
[32] J. Riesch, J.Y. Buffiere, T. Höschen, M. di Michiel, M. Scheel, C. Linsmeier, J.H. You, In situ synchrotron tomography estimation of toughening effect by semi-ductile fibre reinforcement in a tungsten-fibre-reinforced tungsten composite system, Acta Materialia, 61 (2013) 7060-7071.